

NULL-VALIDATED TOPOLOGICAL SIGNATURES OF FINANCIAL MARKET DYNAMICS

SAMUEL W. AKINGBADE[✉]

ABSTRACT. Financial markets exhibit temporal organization that is not fully captured by volatility measures or linear correlation structure. We study a null validated topological approach for quantifying market complexity and apply it to Bitcoin daily log returns. The analysis uses the L^1 norm of persistence landscapes computed from sliding-window delay embeddings. This quantity shows strong co-movement with stochastic volatility during periods of market stress, but remains intermittently elevated during low volatility regimes, indicating dynamical structure beyond fluctuation scale. Rolling correlation analysis reveals that the dependence between geometry and volatility is not stationary. Surrogate based null models provide statistical validation of these observations. Rejection of shuffle surrogates rules out explanations based on marginal distributions alone, while departures from phase randomized surrogates indicate sensitivity to nonlinear and phase dependent temporal organization beyond linear correlations. These results demonstrate that persistence landscape norms provide complementary information about market dynamics across market conditions.

1. INTRODUCTION

Understanding the complex temporal dynamics of financial markets remains a central challenge in financial mathematics, quantitative finance, and econometrics. Traditional tools such as volatility estimates and linear correlation measures provide essential but limited perspectives on market behavior, particularly during periods of stress or structural change. Volatility, often modeled through stochastic processes, captures the scale of fluctuation but may fail to detect subtler dynamical features that reflect temporal organization or higher order dependencies in return series. As a result, there is growing interest in methods that can extract richer information about the geometry and temporal structure of financial time series beyond conventional statistical summaries.

In recent years, topological data analysis (TDA) has emerged as a promising framework for studying the shape of complex data. TDA seeks to describe intrinsic structural features that persist across multiple scales, leveraging tools from algebraic topology to quantify connectivity and loops in point clouds or time series embeddings. At the heart of TDA is persistent homology, a method for tracking the birth and death of topological features such as connected components and cycles as a scale parameter varies,

yielding descriptors like barcodes and persistence diagrams that summarize data shape in a multiscale manner. Persistent homology has been applied across diverse domains where structure matters, including the analysis of complex biological and dynamical signals, due to its robustness to noise and coordinate-free characterization of data geometry; see, for example, [1].

In the context of time series, a common approach is to convert sequential observations into a delay or sliding window embedding that reconstructs the dynamics of the underlying process in a higher-dimensional space. This method draws on ideas related to Takens' embedding theorem [2] and has been studied in both theoretical and applied settings; by embedding a signal into a point cloud in a reconstructed state space, one can apply persistent homology to detect recurrent geometric patterns such as loops and voids that correspond to underlying dynamical phenomena [3]. Practical summaries of these persistent features include persistence landscapes and their norms, which are scalar functions that quantify the prominence of topological features and enable statistical comparison across time.

Application of these methods to financial time series has grown in recent years. A major work by [4] used persistent homology to analyze major U.S. stock indices, showing that persistence landscape norms increase before and during market meltdowns, thereby providing a novel signal that goes beyond standard volatility measures. More recently, [5] offered a theoretical explanation for this behavior by linking the growth of persistence landscape norms to log-periodic power law singularity dynamics, which are commonly used to model speculative bubbles and critical transitions. They showed that when a financial time series follows such dynamics, its delay coordinate embedding naturally exhibits structured oscillatory geometry, leading to the emergence of persistent loop-like features in the reconstructed state space. In a related line of work, [6] developed a topological framework for recognizing critical transitions in cryptocurrency markets, including Bitcoin and Ethereum, in the period leading up to the 2018 market crash. Additional studies have applied topological methods to financial time series in a variety of settings, including early warning detection, critical transitions, bubble identification, sparse portfolio and structural analysis of market dynamics; see, for example, [7, 8, 9, 10, 11, 12, 13].

Subsequent research has applied topological methods to change point detection in financial markets, demonstrating that persistent homology features can align with major economic events and volatility regimes across different stock markets [14]. Persistence landscape norms have been shown to correlate with volatility and uncertainty in financial markets [15, 16], however the dynamical origin of this signal and its dependence on temporal ordering and nonlinear structure remain largely unexplored. These contributions illustrate the potential of persistent homology to capture aspects of market dynamics that are not fully accessible via conventional statistical tools.

Despite these advances, several gaps remain in the rigorous validation and interpretation of topological summaries in financial settings. In particular, it is important to distinguish genuine temporal organization from artifacts of marginal distributions or linear correlation structure. Null model frameworks that systematically test the dependence of topological features on temporal ordering or nonlinear dynamics are less commonly explored, yet they are crucial for establishing statistical significance and interpretability. Addressing this need is especially relevant in markets characterized by regime shifts, such as cryptocurrency markets, which have been widely studied due to their pronounced volatility, behavioral effects, and rapid structural changes [17, 18, 19]. Bitcoin, as the largest and most liquid cryptocurrency, provides a natural setting for examining these issues. Our work contributes to this literature by introducing a null-validated topological analysis of Bitcoin log returns that explicitly compares topological summary statistics to surrogate ensembles designed to preserve specific statistical properties of the series while destroying temporal dependence.

In this study, we investigate the geometric and temporal structure of Bitcoin log return dynamics through a topological lens, treating the L^1 norm of persistence landscapes computed from sliding window delay embeddings as a quantitative summary of reconstructed state-space geometry. Rather than interpreting this quantity solely as a proxy for market stress, we examine how it relates to and differs from established scale-based models of market variability. To this end, a central contribution of this work is a systematic comparison between the persistence landscape norm and filtered stochastic volatility estimates, including an analysis of their time varying association through rolling correlations. This comparison allows us to characterize regimes in which topological structure and volatility align, as well as regimes in which they decouple.

A second central contribution is the incorporation of surrogate-based null models to rigorously assess the statistical origin of the observed topological signal. By employing both shuffle surrogates, which preserve the marginal distribution of returns while destroying temporal ordering, and phase-randomized surrogates, which preserve linear second order structure while removing nonlinear and phase-dependent dependencies, we disentangle the respective roles of marginal effects, linear correlations, and higher order temporal organization. This framework enables us to distinguish genuine geometric structure in the reconstructed dynamics from artifacts induced by distributional or linear properties of the time series.

Our results show that while the persistence landscape norm co-moves strongly with stochastic volatility during periods of market stress, the dependence between the two is not stationary. In particular, the topological signal exhibits intermittent bursts and sustained deviations from baseline even during low-volatility regimes, indicating the presence of organized temporal dynamics that are not captured by fluctuation scale or linear correlation structure alone. Together, these findings position the persistence landscape

norm as a null-validated descriptor of financial time series that is sensitive to volatility and complements stochastic volatility models, providing insight into regime dependent organization in complex market dynamics.

The structure of the paper is as follows. Section 2.1 reviews topological data analysis with a focus on persistent homology, and Section 2.2 describes its application to financial time series, including Bitcoin log returns and the distribution of topological signals across sentiment regimes. Section 3 compares the norm of the persistence landscape obtained from sliding window delay embeddings of log returns with filtered stochastic volatility and examines their rolling correlation. Section 4 introduces surrogate-based null models for statistical validation of the persistence landscape norm as a descriptor of market dynamics beyond volatility and sentiment effects. The main contributions are presented in Sections 3 and 4. Conclusions and future directions are presented in Section 5.

2. BACKGROUND

2.1. Persistent homology. In this section, we describe the topological framework used throughout the paper, based on persistent homology. The tool provides a multiscale characterization of the geometry of point clouds derived from time series and allows us to extract robust numerical summaries of their evolving structure via persistence landscapes. The mathematical foundations of persistent homology and persistence landscapes are well established; see, for example, [20, 21, 22, 23].

2.1.1. Persistent homology. It associates to a finite point cloud a family of topological spaces indexed by a resolution parameter, and tracks the evolution of topological features, such as connected components and loops, across scales. Persistence landscapes provide a functional representation of this multiscale information in a Banach space, enabling numerical summaries and statistical comparison. In this work, we ultimately summarize each point cloud by a single scalar quantity given by the L^1 norm of its persistence landscape.

Let

$$X = \{x_0, x_1, \dots, x_{m-1}\} \subset \mathbb{R}^N$$

be a finite point cloud embedded in Euclidean space. To associate a topological space to X , we consider the Vietoris–Rips construction. For a fixed resolution parameter $t > 0$, the *Vietoris–Rips simplicial complex* $VR(X, t)$ is defined by including a k -simplex with vertices $\{x_{i_0}, \dots, x_{i_k}\}$ whenever the pairwise distances between all vertices are strictly less than t , that is,

$$d^X(x_{i_j}, x_{i_{j'}}) < t \quad \text{for all } x_{i_j}, x_{i_{j'}} \in \{x_{i_0}, \dots, x_{i_k}\}.$$

Intuitively, simplices are added whenever their vertices become indistinguishable at resolution t . As t increases, these complexes form a nested sequence

$$VR(X, t) \subseteq VR(X, t') \quad \text{for } t < t',$$

which constitutes a *filtration* of simplicial complexes.

At each resolution level, we compute the simplicial *homology groups*

$$H_n(VR(X, t))$$

with coefficients in a fixed field, here taken to be \mathbb{Z}_2 . The generators of these groups correspond to n -dimensional topological features: connected components for $n = 0$, loops for $n = 1$, voids for $n = 2$, and so forth. In this work we restrict attention to one-dimensional homology, $n = 1$, so that the analysis focuses exclusively on loop-like geometric structures in the embedded data.

The filtration of simplicial complexes induces a corresponding filtration of homology groups,

$$H_n(VR(X, t)) \hookrightarrow H_n(VR(X, t')) \quad \text{for } t < t',$$

via canonical homomorphisms. This is called a *persistence module*. Persistence modules are uniquely decomposable into a direct sum of interval modules up to permutations [24]. The collection of these indecomposables is referred to as a barcode where the intervals are bars, each representing the evolution of a topological feature (n -dimensional hole).

2.1.2. Persistence diagrams. A homology class $\alpha \in H_n$ is said to be born at scale b_α if it first appears at $t := b_\alpha$ and is not in the image of any class from smaller scales. The class persists across intermediate resolutions and is said to die at scale $d_\alpha > b_\alpha$ if its image becomes trivial at $t := d_\alpha$. Each such class is therefore associated with a birth–death pair (b_α, d_α) , with finite multiplicity determined by the number of classes sharing the same birth and death values. The collection of all birth–death pairs arising from H_n is encoded in the *persistence diagram* P_n , which is a locally finite multiset of points supported on $U := \{(t_1, t_2) \in \mathbb{R}^2 : t_1 < t_2\}$ together with points on the diagonal $\delta U := \{(t, t) \in \mathbb{R}^2\}$ counted with infinite multiplicity, representing trivial features. The horizontal axis corresponds to birth values and the vertical axis to death values.

2.1.3. Persistence landscapes. To obtain a functional representation suitable for numerical analysis, we map persistence diagrams into a Banach space using persistence landscapes.

For each off-diagonal point $(b_\alpha, d_\alpha) \in P_n$, we define the piecewise linear function

$$(2.1) \quad f_{(b_\alpha, d_\alpha)}(x) = \begin{cases} x - b_\alpha, & x \in (b_\alpha, \frac{b_\alpha + d_\alpha}{2}], \\ d_\alpha - x, & x \in (\frac{b_\alpha + d_\alpha}{2}, d_\alpha), \\ 0, & \text{otherwise.} \end{cases}$$

Given a persistence diagram with finitely many off-diagonal points, the *persistence landscape* is defined as the sequence of functions

$$(2.2) \quad \lambda_n = (\lambda_n(i))_{i \in \mathbb{N}}, \quad \lambda_n(i)(x) = i_{\max}\{f_{(b_\alpha, d_\alpha)}(x) \mid (b_\alpha, d_\alpha) \in P_n\},$$

where i_{\max} denotes the i -th largest value among the indicated functions. If the i -th largest value does not exist, $\lambda_n(i)(x)$ is set to zero. The resulting object lies in the Banach space $L^p(\mathbb{N} \times \mathbb{R})$ for any $p \geq 1$.

For a persistence landscape λ_n , the L^p norm is defined by

$$(2.3) \quad \|\lambda_n\|_p = \left(\sum_{i=1}^{\infty} \|\lambda_n(i)\|_p^p \right)^{1/p}, \quad \|\lambda_n(i)\|_p = \left(\int_{\mathbb{R}} |\lambda_n(i)(x)|^p dx \right)^{1/p}.$$

In this work, we focus exclusively on the L^1 norm. For finite persistence diagrams, this norm admits the closed-form expression [21]

$$(2.4) \quad \|\lambda_n\|_1 = \frac{1}{4} \sum_{\alpha} (d_{\alpha} - b_{\alpha})^2.$$

In practice, we compute a numerically approximated and truncated version of this quantity by integrating the first i_{\max} landscape layers over a finite grid of scale values.

2.2. Application to time series. We now describe how this framework is applied to financial time series following [5, 6, 25].

Let

$$Z = \{z_0, z_1, \dots, z_{N-1}\}$$

be a real valued time series of length N . Fix an embedding dimension m and a time delay $d \geq 1$. The delay-coordinate embedding produces a sequence of vectors

$$x_t = (z_t, z_{t+d}, \dots, z_{t+(m-1)d}),$$

defined for all indices t such that the coordinates exist.

2.2.1. Choice of embedding dimension and delay. The use of delay-coordinate embeddings in this work is motivated by classical results from nonlinear dynamical systems theory, which establish conditions under which the geometry of an underlying state space can be reconstructed from time-delayed observations.

A foundational result is *Takens'* embedding theorem [2]. Consider a discrete-time dynamical system $x_{t+1} = T(x_t)$ evolving on a compact smooth manifold M of dimension D , together with a smooth observation function $h : M \rightarrow \mathbb{R}$. Let $\{z_t\}$ be the scalar time series defined by $z_t = h(x_t)$. For a fixed delay $d \geq 1$, define the delay-coordinate map

$$\Phi : M \rightarrow \mathbb{R}^m, \quad \Phi(x_t) = (z_t, z_{t+d}, \dots, z_{t+(m-1)d}).$$

Takens' theorem states that, provided $m \geq 2D + 1$, it is a generic property of the pair (T, h) that Φ is an embedding, i.e., a smooth injective map with a smooth inverse onto its image. In this sense, the delay-coordinate vectors provide a faithful geometric representation of the underlying state space.

This result was subsequently generalized by [26], who showed that if the dynamics admit a compact attractor $A \subset M$ of finite fractal dimension D , then an embedding of the attractor can be achieved for $m \geq 2D + 1$ under

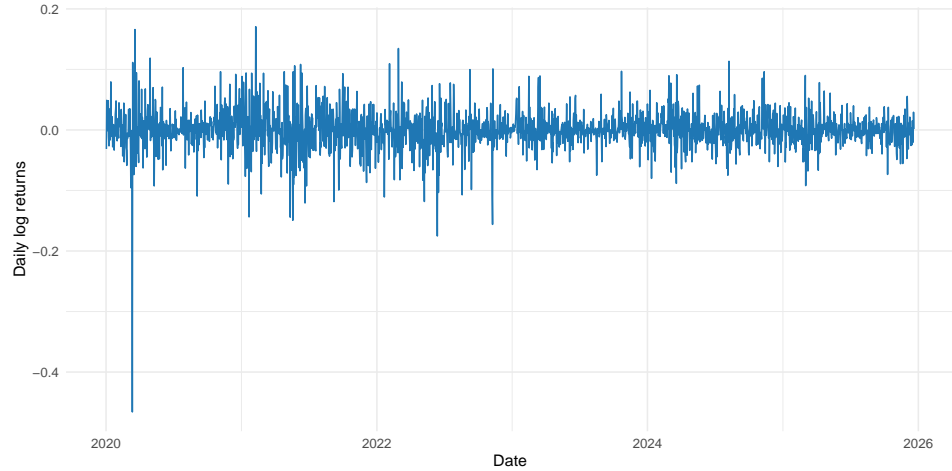


FIGURE 1. Bitcoin daily log returns.

the weaker assumption of prevalence rather than genericity. This extension is particularly relevant in practical settings where the dynamics evolve on a lower dimensional invariant set.

In the present study, delay coordinate embeddings are employed not for exact state-space reconstruction, but as a geometric representation from which topological features can be extracted robustly via persistent homology. Consequently, the embedding dimension m and delay τ are chosen empirically to be sufficient for capturing loop-like geometric structure in the delay embedding while remaining computationally tractable.

2.2.2. Topological summaries of Bitcoin log return dynamics. To detect temporal variation in topological signal, we apply a sliding window of length w to the sequence $\{x_t\}$, yielding a time-indexed family of point clouds

$$X^t = \{x_t, x_{t+1}, \dots, x_{t+w-1}\}.$$

For each window X^t , we compute the Vietoris–Rips filtration, extract the one dimensional persistence diagram, construct the corresponding persistence landscape, and evaluate the truncated L^1 landscape norm.

Bitcoin price data from January 1, 2020 to December 20, 2025 were obtained from Yahoo Finance [27] and used to compute daily log returns shown in Figure 1. The topological data analysis procedure described above is then applied to the standardized Bitcoin log returns.

The result is a scalar time series

$$t \mapsto \|\lambda^t\|_1,$$

which quantifies the evolving prominence of loop-like geometric structure in the embedded dynamics.

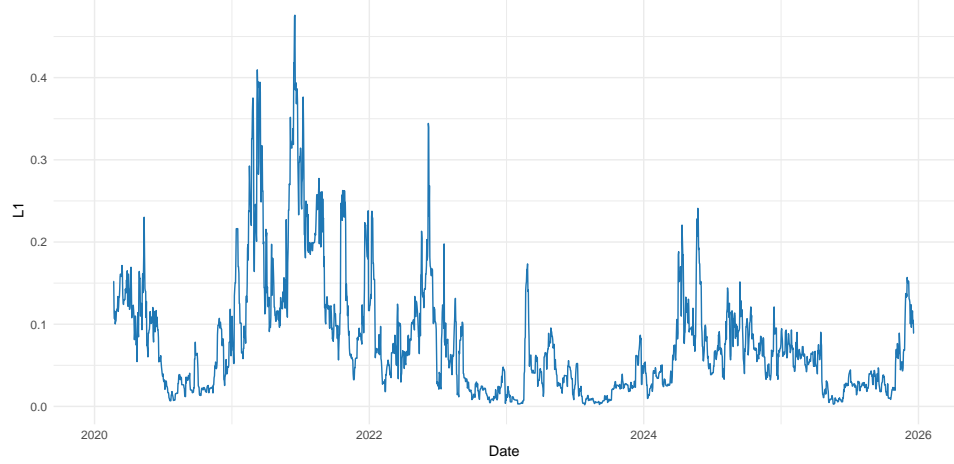


FIGURE 2. L^1 norm of the persistence landscape of Bitcoin log returns.

We show the time evolution of the L^1 norm of the H_1 persistence landscape computed from sliding window delay embeddings of standardized Bitcoin log returns in Figure 2, using an embedding dimension of 4, a delay of 2 and a sliding window of length 50.

The resulting series exhibits multiple intervals of elevated L^1 values throughout the sample, reflecting the recurrence of loop-like geometric structure in the delay space across several distinct periods. These elevated intervals are interspersed with lower activity regimes, indicating that the strength of the topological signal varies over time rather than remaining uniformly high. This temporal variability motivates examining whether the observed topological signal can be explained by conventional market descriptors such as sentiment or volatility.

2.2.3. Distribution of L^1 norms across sentiment regimes. Having established how the L^1 norm of the persistence landscape computed from sliding-window delay embeddings of Bitcoin log returns evolves over time (Figure 2), we now examine how this quantity distributes across sentiment regimes.

Sentiment data were sourced from the Crypto Fear & Greed Index via the public API provided by alternative.me [28]. This index is a composite sentiment indicator scaled between 0 (Extreme Fear) and 100 (Extreme Greed), designed to capture aggregate market sentiment by combining multiple behavioral and market-based inputs, including price momentum, volatility, trading volume, and social media activity.

Figure 3 summarizes the empirical distribution of the L^1 norm, conditioned on contemporaneous Fear & Greed sentiment regimes. While the distributions exhibit substantial overlap, systematic differences in median and dispersion are evident across regimes. In particular, Extreme Fear and

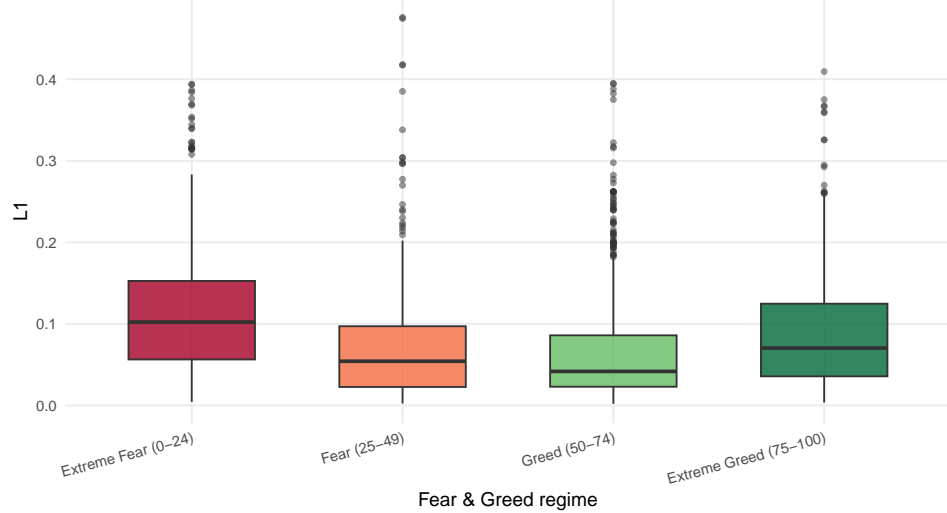


FIGURE 3. Distribution of L^1 norms of the persistence landscape for Bitcoin log returns across Fear & Greed sentiment regimes.

Extreme Greed are associated with elevated central tendencies relative to intermediate sentiment states, though pronounced outliers occur in all categories. Overall, the results indicate that the L^1 norm of the persistence landscape varies across sentiment regimes in a distributional sense, without exhibiting a simple monotonic dependence on sentiment.

3. STOCHASTIC VOLATILITY MODELING OF BITCOIN LOG RETURNS

3.1. Stochastic volatility model. We model the Bitcoin log return series using a standard stochastic volatility (SV) specification, in which the latent state corresponds to the log variance of returns. Let h_t denote the latent log variance at time t . The model is defined by the following two equations.

3.1.1. State (process) equation. The latent log variance follows a mean reverting AR(1) process,

$$(3.1) \quad h_t = \mu + \phi(h_{t-1} - \mu) + \sigma_\eta \eta_t, \quad \eta_t \stackrel{\text{iid}}{\sim} \mathcal{N}(0, 1).$$

where μ is the long run mean of the log variance, $\phi \in (0, 1)$ controls persistence, and $\sigma_\eta > 0$ governs the magnitude of stochastic shocks to the log variance.

We restrict $\phi \in (0, 1)$ to ensure that the latent log variance process is strictly stationary, yielding a well defined long-run distribution for volatility. Under this formulation, crash-related volatility spikes are accommodated through the stochastic innovations η_t and magnified by the exponential mapping, rather than through a globally explosive parameterization of the latent state. This specification captures the high persistence and mean

reverting behavior of volatility observed in financial markets over long horizons without implying permanent divergence from the long-run mean.

3.1.2. *Observation (measurement) equation.* Conditional on h_t , returns are Gaussian with zero mean and variance $\exp(h_t)$,

$$z_t \mid h_t \sim \mathcal{N}(0, \exp(h_t))$$

Under this formulation, $\exp(h_t)$ represents the conditional variance of returns and $\exp(h_t/2)$ the conditional volatility. This specification corresponds to the canonical discrete-time stochastic volatility model widely used in empirical finance (e.g.,[29, 30, 31, 32, 33]).

3.2. Inference and parameter estimation. The SV model is cast as a partially observed Markov process (state-space model) and fitted using likelihood methods based on Monte Carlo sampling. Inference is carried out within the pomp framework, which supports likelihood evaluation and parameter estimation via simulation for nonlinear state-space models with non Gaussian noise.

To enforce parameter constraints during optimization, the model is reparameterized internally so that σ_η is estimated on the log scale and ϕ on the logit scale, ensuring $\sigma_\eta > 0$ and $\phi \in (0, 1)$ throughout estimation.

Initial parameter values are chosen heuristically. In particular, the long run mean μ is initialized using the logarithm of the empirical variance of the return series, while the remaining parameters are set to plausible values reflecting high persistence in financial volatility.

Model parameters $\theta = (\mu, \phi, \sigma_\eta, h_0)$ are estimated by maximum likelihood using iterated filtering (IF2), a simulation-based algorithm for partially observed Markov processes [34, 35]. Iterated filtering repeatedly applies a particle filter while perturbing parameters via a random walk with gradually decreasing variance, allowing the algorithm to ascend the likelihood surface of the state-space model.

For robustness against local maxima and Monte Carlo variability, the estimation procedure is repeated multiple times from the same initial parameter guess. For each replicate, the log-likelihood at the final parameter estimate is evaluated several times using independent particle filters. These likelihood evaluations are aggregated using a numerically stable log-mean-exp operation, which approximates the logarithm of the average likelihood, yielding a single likelihood score per replicate. The parameter set associated with the highest aggregated likelihood is selected as the final estimate $\hat{\theta}$.

3.3. Filtered latent volatility. Given the estimated parameters $\hat{\theta}$, we apply a particle filter to approximate the sequence of filtering distributions

$$p(h_t \mid z_{1:t}; \hat{\theta}), \quad t = 1, \dots, n.$$

The primary quantity of interest is the filtered posterior mean of the latent log variance,

$$\hat{h}_t := \mathbb{E}[h_t \mid z_{1:t}; \hat{\theta}].$$

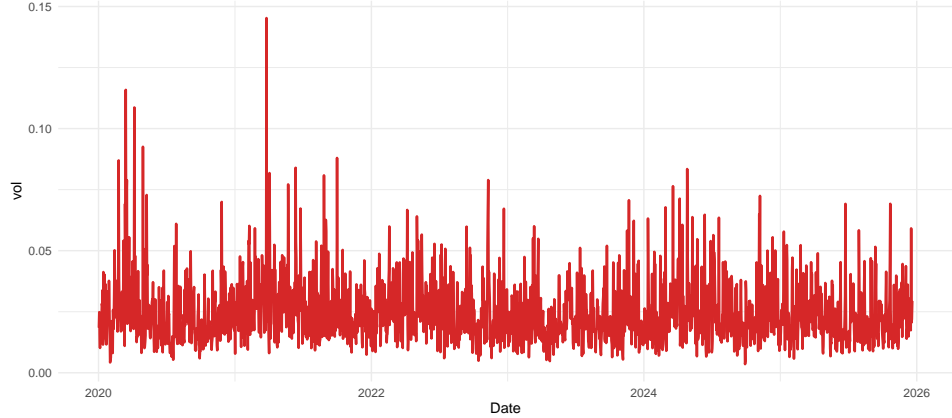


FIGURE 4. Filtered conditional volatility estimate $\hat{\sigma}_t$ obtained from the stochastic volatility model of Bitcoin log returns.

In practice, this expectation is approximated using the particle representation returned by the filter,

$$\hat{h}_t \approx \frac{1}{N_p} \sum_{i=1}^{N_p} h_t^{(i)},$$

where $h_t^{(i)}$ denotes the i -th particle at time t after resampling.

From the filtered log variance sequence $\{\hat{h}_t\}$, we construct estimates of the conditional variance and volatility as

$$(3.2) \quad \hat{V}_t = \exp(\hat{h}_t), \quad \hat{\sigma}_t = \sqrt{\hat{V}_t} = \exp\left(\frac{\hat{h}_t}{2}\right).$$

The resulting series $(\hat{h}_t, \hat{V}_t, \hat{\sigma}_t)$ provides a time-resolved estimate of latent stochastic volatility. Figure 4 displays the filtered volatility series over calendar time, which serves as a latent volatility benchmark for subsequent analysis.

Having obtained a filtered estimate of latent stochastic volatility, we now empirically compare its temporal evolution with the L^1 norm of the persistence landscape computed from sliding-window embeddings of Bitcoin log returns.

3.4. Empirical comparison with topological signal. In Figure 5, we present a standardized comparison between the L^1 norm of the persistence landscape computed from the Bitcoin log return series $\{z_t\}$ and the filtered stochastic volatility estimate.

In early 2020, the onset of the COVID-19 crisis is marked by an abrupt and extreme surge in stochastic volatility. During this period, the topological signal rises as well, indicating that the large amplitude fluctuations

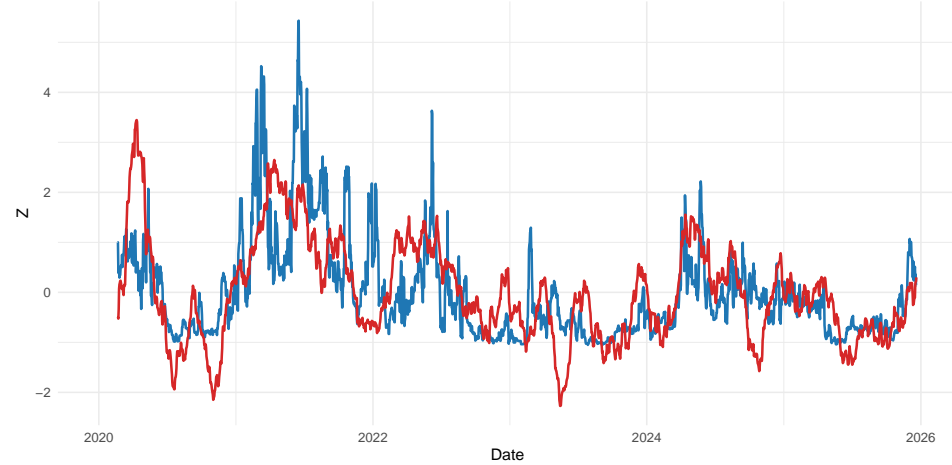


FIGURE 5. Standardized comparison of the L^1 norm of persistence landscape (blue) and filtered stochastic volatility (red).

associated with the market crash are accompanied by pronounced geometric organization in the reconstructed return dynamics. This co-movement persists throughout much of 2020–2021, a period characterized by repeated volatility spikes and sustained market stress, during which both measures remain elevated and closely aligned.

Following these stress episodes, the series enter multiple phases of volatility compression. In mid 2020 and again in late 2020, the standardized volatility drops to values near -2 , indicating unusually low volatility relative to its long-run mean. During these intervals, the topological signal also declines below its mean, but typically not to the same extent as volatility. Furthermore, following the late 2021 to early 2022 decline in market volatility, the stochastic volatility estimate remains suppressed, whereas the topological signal continues to display intermittent bursts and sustained deviations from baseline. This asymmetric relaxation suggests that while fluctuation amplitude contracts rapidly after major shocks, geometric organization in return dynamics decays more gradually, retaining some structure even as volatility becomes unusually subdued.

A similar but more prolonged compression regime occurs in 2023. In standardized units, stochastic volatility remains persistently suppressed for an extended period, reaching values near -2 and exhibiting relatively little variation. Over the same interval, the topological signal is often negative as well, but again does not compress as strongly and continues to display intermittent excursions. This behavior indicates that periods of apparent market calm, as measured by volatility, can still be associated with nontrivial temporal organization in returns, though at a reduced level compared to crisis periods.

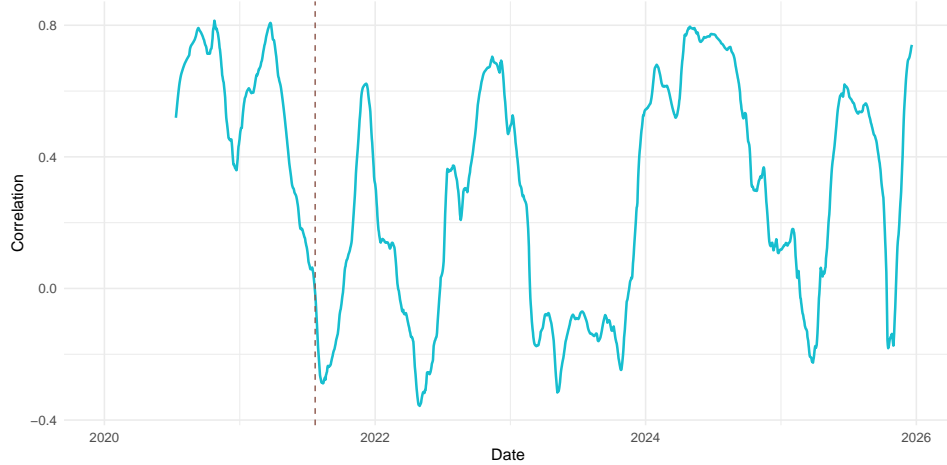


FIGURE 6. Rolling correlation between the L^1 norm and stochastic volatility (180-day window).

All these observations indicate two key features. First, during periods of severe market stress, volatility and topological signal rise together reflecting the joint presence of large fluctuations and strong geometric structure. Second, outside these regimes, particularly during volatility compression phases, the relationship becomes asymmetric: volatility often contracts more strongly and more rapidly than the topological signal. This indicates that the L^1 norm is sensitive not only to fluctuation scale but also to the persistence and organization of return dynamics, which can survive, albeit in weakened form, during extended periods of low volatility.

To quantify the evolving relationship between topological signal and volatility, we examine the rolling correlation between the L^1 norm and the filtered stochastic volatility estimate over a 180-day horizon in Figure 6. At each time point, the curve reports the linear association between topology and volatility over the preceding six months, providing a time-resolved measure of their dependence.

During periods of heightened market stress, the rolling correlation attains sustained positive values, indicating that increases in volatility are accompanied by concurrent increases in topological signal. This behavior is consistent with the co-movement observed in Figure 5 during crisis regimes, where large-amplitude fluctuations and strong geometric organization arise together.

In contrast, following the subsequent contraction in volatility, the rolling correlation undergoes a pronounced decline and becomes markedly unstable, with extended intervals of weak or even negative association. Although the correlation exhibits multiple local minima, changepoint detection using the Pruned Exact Linear Time (PELT) algorithm identifies a single dominant shift (indicated by the brown dashed line in Figure 6) in the mean level of

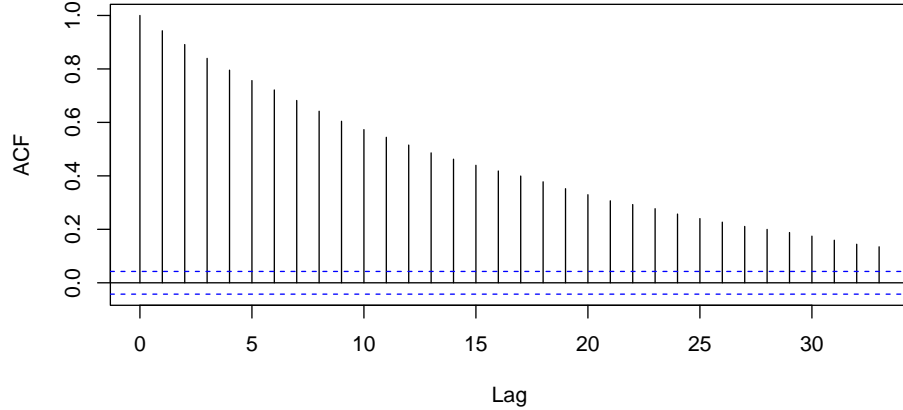


FIGURE 7. ACF of the residual L^1 norm of the persistence landscape computed from Bitcoin log return embeddings after removing linear effects of stochastic volatility and sentiment.

dependence. This transition separates an earlier regime characterized by persistently strong coupling from a later regime in which the association between topology and volatility is weaker and more variable.

This behavior indicates that the dependence between topological signal and volatility is not stationary over time. While the two measures align closely during crisis periods, the topological signal may persist or exhibit intermittent intensification even as volatility subsides. This further supports the interpretation that the L^1 norm captures aspects of return dynamics beyond fluctuation scale alone, reflecting changes in temporal organization that are not fully encoded by volatility.

3.5. Topological signal beyond volatility and sentiment. We perform a residualization analysis to examine whether the topological signal is fully explained by stochastic volatility and variation in sentiment. In this analysis, the L^1 norm of the persistence landscape computed from delay embeddings of Bitcoin log returns is regressed on contemporaneous measures of volatility and sentiment. Specifically, we consider the linear model

$$(3.3) \quad L_1(t) = \beta_0 + \beta_1 \bar{\sigma}_t + \beta_2 \bar{F}_t + \beta_3 S_t + \varepsilon_t,$$

where $L_1(t)$ denotes the L^1 norm summarizing the topological signal of the log return dynamics, $\bar{\sigma}_t$ is the rolling window mean of the filtered stochastic volatility, \bar{F}_t is the rolling window mean of the Fear & Greed sentiment

index, and $S_t := \sqrt{\text{Var}(F_{t-L+1:t})}$ denotes the rolling window standard deviation of sentiment. The coefficients β_0, \dots, β_3 capture linear associations between the topological summary and the covariates, while the residual term ε_t represents the component of topological variation not explained by volatility or sentiment.

The primary object of interest is the temporal dependence structure of the residual series ε_t . Figure 7 displays the autocorrelation function (ACF) of ε_t , which exhibits a slow decay with statistically significant correlations persisting across many lags. This behavior is inconsistent with a white noise residual and indicates that structured temporal organization remains in the topological signal after removing linear effects of volatility and coarse sentiment statistics.

4. CONSTRUCTION OF SURROGATE NULL MODELS

Let $\{z_t\}_{t=1}^N$ denote the standardized Bitcoin log return series. To determine whether the L^1 norm of the persistence landscape obtained from sliding window delay embeddings of $\{z_t\}$ arise from genuine temporal structure, rather than effects attributable to the marginal distribution or linear second-order dependence, we compare the resulting time series of persistence landscape norms to those obtained from two classes of surrogate Bitcoin log return processes. Each surrogate is transformed through the same embedding and persistent homology pipeline, thereby inducing a null distribution for the windowed persistence landscape norm defined in 2.1.

4.1. Shuffle (i.i.d.) surrogate. Let π be a random permutation of $\{1, \dots, N\}$ drawn uniformly from the symmetric group S_N . The *shuffle surrogate* of the observed series $\{z_t\}_{t=1}^N$ is defined by

$$(4.1) \quad z_t^s := z_{\pi(t)}, \quad t = 1, \dots, N.$$

This construction preserves the empirical marginal distribution of $\{z_t\}$ exactly, but destroys all temporal ordering and hence all serial dependence. In probabilistic terms, this surrogate corresponds to a null in which the observed series is treated as exchangeable.

For each realization $j = 1, \dots, N_s$, we generate an independent permutation π_j , compute the corresponding surrogate series $z_t^{s,j}$, and apply section 2.1 to obtain a surrogate topological time series.

4.2. FFT phase-randomized surrogate. The second null preserves second order temporal structure while destroying nonlinear and phase dependent features. Let $\tilde{z}_t = z_t - \bar{z}$ denote the demeaned series, and define its discrete Fourier transform (DFT) by

$$(4.2) \quad Z_k := \sum_{t=0}^{N-1} \tilde{z}_t e^{-2\pi i k t / N}, \quad k = 0, \dots, N-1.$$

Write $Z_k = |Z_k|e^{i\theta_k}$. A *phase randomized* surrogate is constructed by replacing the phases θ_k at positive frequencies with i.i.d. random variables

$$(4.3) \quad \phi_k \sim \text{Unif}(0, 2\pi),$$

while retaining the magnitudes $|Z_k|$, and enforcing conjugate symmetry so that the inverse transform is real-valued. Concretely, for $k = 1, \dots, \lfloor (N-1)/2 \rfloor$, define

$$(4.4) \quad Z_k^{\text{fft}} := |Z_k|e^{i\phi_k}, \quad Z_{N-k}^{\text{fft}} := \overline{Z_k^{\text{fft}}},$$

and set $Z_0^{\text{fft}} := Z_0$. If N is even, the Nyquist component $k = N/2$ must be real; one may set $Z_{N/2}^{\text{fft}} := Z_{N/2}$ (or equivalently randomize with a sign change consistent with real-valuedness).

The inverse DFT yields a surrogate demeaned series

$$(4.5) \quad \tilde{z}_t^{\text{fft}} := \frac{1}{N} \sum_{k=0}^{N-1} Z_k^{\text{fft}} e^{2\pi i k t / N}, \quad t = 0, \dots, N-1,$$

to which the original mean \bar{z} is restored via $z_t^{\text{fft}} = \tilde{z}_t^{\text{fft}} + \bar{z}$.

This procedure preserves the power spectrum (and hence the autocovariance function) asymptotically, while destroying higher-order temporal dependencies and nonlinear phase relationships [36, 37]. As before, for each realization $j = 1, \dots, N_{\text{fft}}$, we apply 2.1 to obtain a surrogate topological time series.

4.3. Pointwise null envelopes for persistence landscape norms. For each sliding window, and for each null model, we generate multiple surrogate realizations of the persistence landscape norm by applying the same embedding and topological pipeline in 2.1 to surrogate versions of $\{z_t\}$. These surrogate values form an empirical sample from the null distribution of the window-level statistic. In all experiments, null envelopes are estimated using 30 surrogate realizations per null model. The qualitative behavior of the envelopes and exceedance patterns is robust to further increases in the number of surrogate realizations.

At each window, we summarize this null distribution by computing its mean, as well as its 5th and 95th empirical percentiles. The interval defined by these two percentiles constitutes a pointwise null envelope for the persistence landscape norm at that window.

This envelope provides a marginal comparison at each window index and should not be interpreted as a simultaneous confidence band across time; in particular, it does not control the family-wise error rate over all windows.

4.4. Exceedance statistics. We investigate deviations of the persistence landscape norm from its surrogate-based null envelopes by examining exceedances across sliding windows. We restrict attention to windows for which both the norm computed from the Bitcoin log return series and the corresponding null quantiles are well defined.

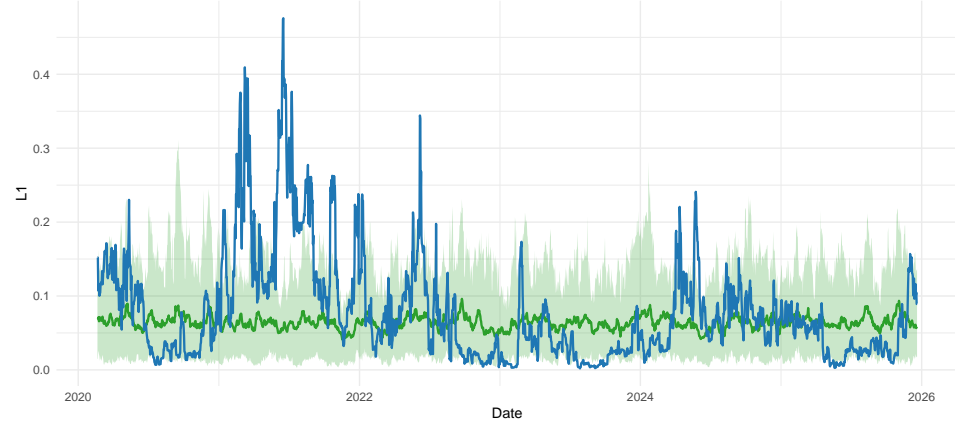


FIGURE 8. Comparison of L^1 norm of the persistence landscape (blue) to pointwise null envelopes obtained from shuffle surrogates.

An exceedance below the null is recorded when the persistence landscape norm falls below the lower (5th percentile) bound of the null envelope, while an exceedance above the null is recorded when it exceeds the upper (95th percentile) bound. We count the total number of such lower and upper exceedances across all valid windows.

Finally, we report the fractions of windows in which the persistence landscape norm lies below or above the null envelope, respectively. These fractions provide a concise summary of how often the observed topological signal deviates from that expected under the surrogate null models.

The empirical behavior of these envelopes and the associated exceedance frequencies are examined in section 4.5.

4.5. Comparison to Surrogate-based null envelopes.

4.5.1. *Shuffle surrogate comparison.* In Figure 8, we compare the observed time series of L^1 norm of the persistence landscape to pointwise null envelopes obtained from shuffle surrogates. Because shuffle surrogates preserve the marginal distribution of returns but destroy all temporal ordering, exceedances relative to this envelope indicate sensitivity of the windowed norms to temporal dependence.

The series frequently exceeds the upper bound of the shuffle null envelope, particularly during pronounced volatility episodes in early 2021 and mid 2022, where the landscape norm rises well above what is expected under random reordering of returns. These excursions indicate that the topological signal captured by the sliding-window embeddings is not explained by the empirical distribution of returns alone and depends critically on temporal ordering.

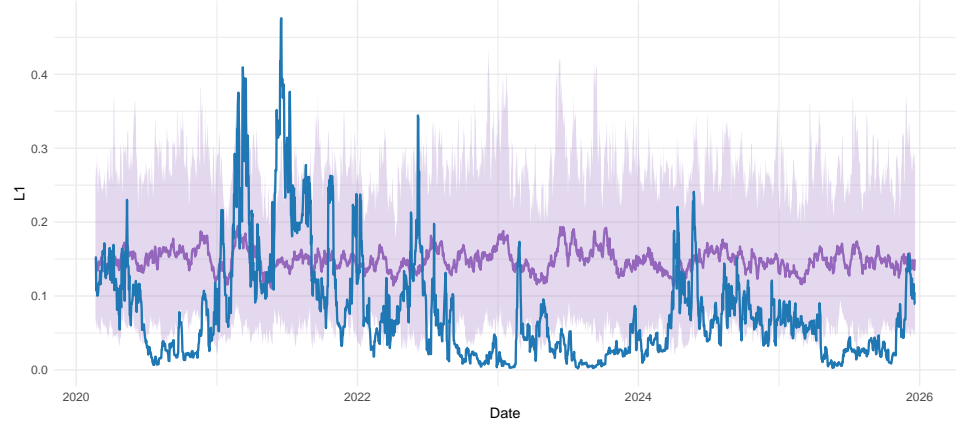


FIGURE 9. Comparison of L^1 norm of the persistence landscape (blue) to null envelopes generated by FFT phase randomized surrogates.

At the same time, there are periods, most notably during relatively calm market regimes, where the norm of the persistence landscape falls within or below the shuffle envelope, suggesting that during these intervals the windowed topological signal is closer to that expected under weak or absent temporal dependence.

The exceedance rates confirm that a non-negligible fraction of windows lie above the 95% shuffle envelope, with rejection frequencies well above the nominal 5% level. This supports rejection of the hypothesis that the norm of the persistence landscapes arises solely from the marginal distribution of Bitcoin log returns.

4.5.2. FFT phase-randomized surrogate comparison. In Figure 9, we compare the observed persistence landscape norm to null envelopes generated by FFT phase randomized surrogates. These surrogates preserve the power spectrum and hence linear second order temporal structure while destroying nonlinear and phase-dependent dependencies.

Relative to this more restrictive null, the norm exhibits a different pattern. While occasional excursions above the FFT envelope occur, they are markedly fewer and more localized than in the shuffle case. In many periods, particularly after 2022, the series lies persistently below the mean of the FFT null ensemble, and often near the lower edge of the envelope.

This behavior indicates that the norm of persistent landscape is sensitive to structure beyond linear correlation alone. The suppression of the norm relative to the FFT null suggests that nonlinear temporal organization present in $\{z_t\}$ constrains the geometry of the delay embedded point clouds in a way that is not reproduced by phase randomized surrogates.

Both of these results demonstrate that the L^1 norm of the persistence landscape derived from Bitcoin log returns exhibits temporal structure that cannot be explained by either the marginal distribution alone or by linear second-order temporal dependence. The shuffle surrogate analysis establishes sensitivity to temporal ordering, while the FFT phase randomized analysis indicates structure beyond that captured by linear correlations.

5. CONCLUSIONS

We introduce a null-validated topological measure for quantifying market complexity and establish that it captures geometric and temporal structure in Bitcoin log return dynamics that is not reducible to sentiment or latent stochastic volatility. The analysis treats the L^1 norm of the persistence landscape derived from sliding-window delay embeddings as a scalar summary of reconstructed state-space geometry and demonstrates its sensitivity to nontrivial temporal organization.

Comparison with filtered stochastic volatility estimates shows that the persistence-landscape norm and volatility encode distinct dynamical information. During high stress regimes, the two quantities exhibit strong positive association, whereas outside these regimes the dependence may weaken and become unstable. Rolling correlation analysis confirms that the coupling between topology and volatility is non-stationary, with a dominant regime shift separating periods of strong alignment from those characterized by weak or fluctuating association. The persistence of elevated topological signal during low volatility intervals implies that geometric organization in delay space is not eliminated by volatility normalization.

Surrogate based null models provide statistical validation of these observations. Rejection of shuffle surrogates demonstrates that the persistence landscape norm depends on temporal ordering and is not determined solely by the marginal distribution of Bitcoin log returns. Departures from FFT phase randomized surrogates further indicate sensitivity to nonlinear and phase dependent temporal dependencies beyond linear second order structure. While the precise mechanisms driving pronounced peaks in the persistence landscape norm remain an open question, the surrogate-based analysis establishes that these features cannot be explained by marginal distributions or linear correlation structure alone.

Overall, the analysis establishes the L^1 norm of the persistence landscape as a mathematically interpretable and statistically validated descriptor of market dynamics. Nontrivial geometric structure persists in Bitcoin log returns even after accounting for volatility and sentiment effects. This framework provides a principled approach for detecting regime dependent organization in financial time series and suggests that topological methods can reveal coherent dynamical structure in regimes where conventional scale-based measures indicate apparent market calm.

An important direction for future work is the application of the null validated topological framework developed here to other asset classes and financial markets, including major U.S. equity indices, fixed income instruments, and cross-asset systems such as major stock indices and commodity markets. Extending the analysis to these settings would allow for systematic comparison of geometric and temporal organization across market structures and time scales, and would help assess the generality of topological signatures observed in cryptocurrency markets. From a methodological perspective, future work may also incorporate more restrictive surrogate constructions, such as iterated amplitude adjusted Fourier transform surrogates, to further disentangle nonlinear temporal structure from linear dependence and marginal distribution effects.

ACKNOWLEDGEMENT

I would like to thank Marian Gidea for helpful discussions and valuable feedback.

REFERENCES

- [1] Tiago Pereira, Alex Carvalho, Lilo Wahl, and Jürgen Kurths. Persistent homology of time-dependent functional networks constructed from coupled time series. *Chaos: An Interdisciplinary Journal of Nonlinear Science*, 28(3):033103, 2018.
- [2] Floris Takens. Detecting strange attractors in turbulence. In David Rand and Lai-Sang Young, editors, *Dynamical Systems and Turbulence, Warwick 1980*, pages 366–381, Berlin, Heidelberg, 1981. Springer Berlin Heidelberg.
- [3] Jose A Perea and John Harer. Sliding windows and persistence: An application of topological methods to signal analysis. *Foundations of Computational Mathematics*, 15(3):799–838, 2015.
- [4] Marian Gidea and Yuri Katz. Topological data analysis of financial time series: Landscapes of crashes. *Physica A: Statistical Mechanics and its Applications*, 491:820–834, 2018.
- [5] Samuel W. Akingbade, Marian Gidea, Matteo Manzi, and Vahid Nateghi. Why topological data analysis detects financial bubbles? *Communications in Nonlinear Science and Numerical Simulation*, 2024.
- [6] Marian Gidea, Daniel Goldsmith, Yuri Katz, Pablo Roldan, and Yonah Shmalo. Topological recognition of critical transitions in time series of cryptocurrencies. *Physica A: Statistical Mechanics and its Applications*, 548:123843, 2020.
- [7] Stelios Arvanitis and Michalis Detsis. Mild explocivity, persistent homology and cryptocurrencies' bubbles: An empirical exercise. *AIMS Mathematics*, 9(1):896–917, 2024.
- [8] Mohd Sabri Ismail, Mohd Salmi Md Noorani, Munira Ismail, Fatimah Abdul Razak, and Mohd Almie Alias. Early warning signals of financial crises using persistent homology. *Physica A: Statistical Mechanics and its Applications*, 586:126459, 2021.
- [9] Marian Gidea. Topological data analysis of critical transitions in financial networks. In *International conference and school on network science*, pages 47–59. Springer, 2017.
- [10] Anubha Goel, Puneet Pasricha, and Juho Kannainen. Risk reduced sparse index tracking portfolio: A topological data analysis approach. *Omega*, 138:103432, 2026.
- [11] Anubha Goel, Damir Filipović, and Puneet Pasricha. Sparse portfolio selection via topological data analysis based clustering. *Quantitative Finance*, 25(8):1261–1291, 2025.

- [12] Rodrigo Rivera-Castro, Polina Pilyugina, and Evgeny Burnaev. Topological data analysis for portfolio management of cryptocurrencies. In *2019 International Conference on Data Mining Workshops (ICDMW)*, pages 238–243. IEEE, 2019.
- [13] P. Saengduean, S. Noisagool, and F. Chamchod. Topological data analysis for identifying critical transitions in cryptocurrency time series. In *2020 IEEE International Conference on Industrial Engineering and Engineering Management (IEEM)*, pages 933–938, 2020.
- [14] Jian Yao, Jingyan Li, Jie Wu, Mengxi Yang, and Xiaoxi Wang. Change point detection in financial market using topological data analysis. *Systems*, 13(10):875, 2025.
- [15] Simon Rudkin, Wanling Qiu, and Paweł Dłotko. Uncertainty, volatility and the persistence norms of financial time series. *arXiv preprint arXiv:2110.00098*, 2021.
- [16] Hugo Gobato Souto. Topological tail dependence: Evidence from forecasting realized volatility. *The Journal of Finance and Data Science*, 9:100107, 2023.
- [17] Brahim Gaies, Mohamed Sahbi Nakhli, Jean-Michel Sahut, and Denis Schweizer. Interactions between investors’ fear and greed sentiment and bitcoin prices. *The North American Journal of Economics and Finance*, 67:101924, 2023.
- [18] Mengxi He, Lihua Shen, Yaojie Zhang, and Yi Zhang. Predicting cryptocurrency returns for real-world investments: A daily updated and accessible predictor. *Finance Research Letters*, 58:104406, 2023.
- [19] Jying-Nan Wang, Hung-Chun Liu, and Yuan-Teng Hsu. A u-shaped relationship between the crypto fear-greed index and the price synchronicity of cryptocurrencies. *Finance Research Letters*, 59:104763, 2024.
- [20] Herbert Edelsbrunner and John L Harer. *Computational topology: an introduction*. American Mathematical Society, 2022.
- [21] Peter Bubenik et al. Statistical topological data analysis using persistence landscapes. *J. Mach. Learn. Res.*, 16(1):77–102, 2015.
- [22] Peter Bubenik and Paweł Dłotko. A persistence landscapes toolbox for topological statistics. *Journal of Symbolic Computation*, 78:91–114, 2017.
- [23] Peter Bubenik. The persistence landscape and some of its properties, 2018.
- [24] Afra Zomorodian and Gunnar Carlsson. Computing persistent homology. *Discrete & Computational Geometry*, 33(2):249–274, 2005.
- [25] Samuel W. Akingbade. *Applications of Dynamical Systems in Dissipative Mechanics and in Topological Data Analysis*. PhD thesis, Yeshiva University, New York, 2024.
- [26] Sauer Tim, A Yorke James, and Casdagli Martin. Embedology. *Journal of Statistical Physics*, 65(3-4):579–616, 1991.
- [27] Yahoo finance. <https://finance.yahoo.com/>. Accessed December, 2025.
- [28] Alternative.me. <https://alternative.me/crypto/api/>. Accessed December, 2025.
- [29] Stephen J. Taylor. *Modelling Financial Time Series*. John Wiley & Sons, Chichester, 1986.
- [30] Andrew C. Harvey, Esther Ruiz, and Neil Shephard. Multivariate stochastic variance models. *Review of Economic Studies*, 61(2):247–264, 1994.
- [31] Sangjoon Kim, Neil Shephard, and Siddhartha Chib. Stochastic volatility: Likelihood inference and comparison with arch models. *Review of Economic Studies*, 65(3):361–393, 1998.
- [32] Neil Shephard. Statistical aspects of arch and stochastic volatility. In D. R. Cox, D. V. Hinkley, and O. E. Barndorff-Nielsen, editors, *Time Series Models in Econometrics, Finance and Other Fields*, pages 1–67. Chapman & Hall, 1996.
- [33] John Hull and Alan White. The pricing of options on assets with stochastic volatilities. *The Journal of Finance*, 42(2):281–300, 1987.
- [34] Edward L. Ionides, Anindya Bhadra, Yves Atchadé, and Aaron A. King. Iterated filtering. *Annals of Statistics*, 39(3):1776–1802, 2011.

- [35] Aaron A. King, Dao Nguyen, and Edward L. Ionides. Statistical inference for partially observed markov processes via the R package pomp. *Journal of Statistical Software*, 69(12):1–43, 2016.
- [36] Thomas Schreiber and Andreas Schmitz. Surrogate time series. *Physica D: Nonlinear Phenomena*, 142(3–4):346–382, 2000.
- [37] James Theiler, Stephen Eubank, André Longtin, Bryan Galdrikian, and J. Doyne Farmer. Testing for nonlinearity in time series: The method of surrogate data. *Physica D: Nonlinear Phenomena*, 58(1–4):77–94, 1992.

DEPARTMENT OF MATHEMATICS, UNIVERSITY OF MICHIGAN, ANN ARBOR, MI, USA.

Email address: `sakingba@umich.edu`.

Email address: `sakingba@mail.yu.edu` (permanent).